2014

A multiwavelength view on the dusty Wolf-Rayet star WR 48a

Svetozar A. Zhekov
Space Research and Technology Institute, Sofia, Bulgaria

Toma Tomov
Nicolaus Copernicus University of Torun

Marcin P. Gawronski
Nicolaus Copernicus University of Torun

Leonid N. Georgiev
Universidad Nacional Autonoma de Mexico

Jura Borissova
Universidad de Valparaiso

See next page for additional authors

Recommended Citation

Zhekov, S. A., Tomov, T., Gawronski, M. P., Georgiev, L. N., Borissova, J., Kurtev, R., Gagne, M., & Hajduk, M. (2014). A multiwavelength view on the dusty Wolf-Rayet star WR 48a. *Monthly Notices of the Royal Astronomical Society, 445*(2), 1663-1678. http://dx.doi.org/10.1093/mnras/stu1880

Authors
Svetozar A. Zhekov, Toma Tomov, Marcin P. Gawronski, Leonid N. Georgiev, Jura Borissova, Radostin Kurtev, Marc Gagne, and Marcin Hajduk

Monthly Notices
of the
ROYAL ASTRONOMICAL SOCIETY
MNRAS **445,** 1663–1678 (2014) doi:10.1093/mnras/stu1880

A multiwavelength view on the dusty Wolf–Rayet star WR 48a★

Svetozar A. Zhekov,[1†] Toma Tomov,[2] Marcin P. Gawronski,[2] Leonid N. Georgiev,[3‡] Jura Borissova,[4,5] Radostin Kurtev,[4,5] Marc Gagné[6] and Marcin Hajduk[7]

[1]*Space Research and Technology Institute, Akad. G. Bonchev str., bl.1, BG-1113 Sofia, Bulgaria*
[2]*Centre for Astronomy, Faculty of Physics, Astronomy and Informatics, Nicolaus Copernicus University, Grudziadzka 5, PL-87-100 Torun, Poland*
[3]*Instituto de Astronomía, Universidad Nacional Autónoma de México, Apartado Postal 70-264, CP 04510 México DF, Mexico*
[4]*Instituto de Física y Astronomía, Facultad de Ciencias, Universidad de Valparaíso, Av. Gran Bretaña 1111, Playa Ancha, Casilla 5030, Valparaíso 2340000, Chile*
[5]*Millennium Institute of Astrophysics, MAS, Santiago, Chile*
[6]*Department of Geology and Astronomy, West Chester University, West Chester, PA 19383, USA*
[7]*Nicolaus Copernicus Astronomical Center, ul. Rabianska 8, PL-87-100 Torun, Poland*

Accepted 2014 September 8. Received 2014 September 8; in original form 2014 August 15

ABSTRACT

We present results from the first attempts to derive various physical characteristics of the dusty Wolf–Rayet (WR) star WR 48a based on a multiwavelength view of its observational properties. This is done on the basis of new optical and near-infrared spectral observations and on data from various archives in the optical, radio and X-rays. The optical spectrum of WR 48a is acceptably well represented by a sum of two spectra: of a WR star of the WC8 type and of a WR star of the WN8h type. The strength of the interstellar absorption features in the optical spectra of WR 48a and the near-by stars D2-3 and D2-7 (both members of the open cluster Danks 2) indicates that WR 48a is located at a distance of ∼4 kpc from us. WR 48a is very likely a thermal radio source and for such a case and smooth (no clumps) wind its radio emission suggests a relatively high mass-loss rate of this dusty WR star ($\dot{M} \approx$ a few $\times\ 10^{-4}$ M$_\odot$ yr^{-1}). Long time-scale (years) variability of WR 48a is established in the optical, radio and X-rays. Colliding stellar winds likely play a very important role in the physics of this object. However, some luminous blue variable like activity could not be excluded as well.

Key words: stars: distances – stars: individual: WR 48a – stars: mass-loss – stars: Wolf–Rayet – radio continuum: stars – X-rays: stars.

1 INTRODUCTION

WR 48a is a carbon-rich (WC) Wolf–Rayet (WR) star that was discovered in a near-infrared (NIR) survey by Danks et al. (1983). It is located inside the G305 star-forming region in the Scutum Crux arm of the Galaxy. Two compact infrared (IR) clusters (Danks 1 and 2) are found in its vicinity (within 2 arcmin) which indicates that this WR star likely originates from one or the other (Danks et al. 1984). The most pronounced characteristics of WR 48a deduced from observations are (a) its optical extinction is very high, $A_V = 9.2$ mag (Danks et al. 1983); (b) it is a strong and variable IR source (e.g. Williams et al. 2012); (c) it is very luminous and variable in X-rays (Zhekov, Gagné & Skinner 2011, 2014).

The IR variability of WR 48a suggests that it is a long-period episodic dust maker with short-term 'flares' superimposed on a much gradually changing emission (Williams 1995; Williams et al. 2003). A recent study revealed a recurrent dust formation on a time-scale of more than 32 yr which also indicates that WR 48a is very likely a wide colliding-wind binary (Williams et al. 2012). However, the case of WR 48a might not be that simple. For example, Hindson et al. (2012) reported detection of a *thermal* radio source (spectral index $\alpha = 0.6$, $F_\nu \propto \nu^\alpha$) associated with WR 48a, while the wide colliding-wind binaries are in general *non-thermal* radio sources (Dougherty & Williams 2000).

Nonetheless, we note that the X-ray properties of WR 48a provide additional support for the binary nature of this WC star. Analysis of the *XMM–Newton* and *Chandra* spectra of WR 48a showed that (Zhekov et al. 2011, 2014): (i) its X-ray emission is of thermal origin; (ii) this is the most X-ray luminous WR star in the Galaxy detected so far, after the black hole candidate Cyg X-3; (iii) the X-ray emission is variable and the same is valid for the X-ray absorption to this object. All these X-ray characteristics are well explained in the framework of the colliding-stellar-wind (CSW) picture although specific information from different spectral domains is yet needed for carrying out a detailed quantitative modelling.

In this study, our goal was to undertake the first attempts to derive various physical characteristics of WR 48a in different

★Based on observations made with the Southern African Large Telescope (SALT) under program 2012_1_POL_OTH_1 (PI: Toma Tomov).
†E-mail: szhekov@space.bas.bg
‡Deceased, 2012 December 26.

spectral domains. To do so, we obtained new optical and near-infrared spectra of WR 48a. Also, we made use of some data from the optical, radio and X-ray archives of various ground-based and space observatories. All this, the new and archival data, allowed us to derive valuable pieces of information on the evolution of the physical characteristics of WR 48a. We could thus start building a global picture of this fascinating object based on a multiwavelength view of its properties. In Section 2, we review the observational information in different spectral domains. In Section 3, we describe our results. We discuss the results from our analysis in Section 4 and list our conclusions in Section 5.

2 OBSERVATIONS AND DATA REDUCTION

2.1 Optical and NIR

We obtained new optical and NIR spectra of WR 48a with the Southern African Large Telescope (SALT; Buckley, Swart & Meiring 2006; O'Donoghue et al. 2006), the 1.9-m telescope at the South African Astronomical Observatory and the New Technology Telescope (NTT) at the European Southern Observatory (ESO). Our search in the archives of various ground-based observatories in the Southern hemisphere found one useful optical observation with the Anglo-Australian Telescope (AAT) at the Anglo-Australian Observatory. We give next some basic information on these data and the corresponding data reduction.

SALT. The SALT spectra of WR 48a were obtained with the Robert Stobie Spectrograph (RSS; Burgh et al. 2003; Kobulnicky et al. 2003) on 2012 May 27. The spectrum of a bright, nearby B star (CPD-62 3058, see Fig. 1) was obtained with the same set-up on 2012 May 24. In the RSS long-slit spectroscopy mode, the volume phase holographic (VPH) gratings PG1800 and PG2300 were used in the spectral range 4000–8800 Å. The whole spectrum in this region was obtained in five shots covering the subregions 4050–5100, 4880–5850, 5810–6670, 6640–7840 and 7790–8840 Å, respectively. Spectra of ThAr, Ne and Xe comparison arcs were obtained to calibrate the wavelength scale. The slit width was 1.5 arcsec and its position on the sky is shown in Fig. 1. The position of the slit was chosen in this way, to be able to obtain the spectra of WR 48a and the WC8 star D2-3 (2MASS J13125770−6240599) simultaneously. As one can see in Fig. 1, four additional stars are well located in the slit and their spectra were also considered in this paper (see Appendix A). The spectral resolution in the particular subregions, estimated by the full widths at the half-maximum (FWHM) of the extracted comparison spectra lines, is as follows: 1.52 ± 0.05, 1.40 ± 0.17, 1.20 ± 0.05, 1.66 ± 0.07 and 1.36 ± 0.05 Å. For the flux calibration, we used spectra of the spectrophotometric standard stars LTT 4364, LTT 7987 and Feige 110, obtained in the nights of 2012 May 24 and 27.

The initial data reduction, including bias and overscan subtraction, gain and cross-talk corrections, trimming and mosaicking, was done with the SALT science pipeline (Crawford et al. 2010). We used the DCR software written by W. Pych (see Pych 2004 for details) to remove the cosmic rays from the observations. To perform the flat-field corrections, the wavelength calibration and to correct the distortion and the tilt of the frames we used the standard IRAF[1] tasks in the TWOSPEC package. The nights of our observations were not photometric. Moreover, SALT is a telescope with a variable pupil which makes the absolute flux calibration impossible. Thus, we calibrated the spectra in relative flux units using an average sensitivity curve. This allowed us to derive the relative spectral energy distribution of the studied objects. The normalized SALT spectra of WR 48a and D2-3 are presented in Fig. 2.

A low-resolution spectrum of WR 48a was acquired on 2013 July 17 with the Grating Spectrograph with a SITe CCD mounted on the 1.9-m Radcliffe telescope at the South African Astronomical Observatory (SAAO). Grating number 7 with 300 lines mm^{-1} and a slit width of 1.5 arcsec were used. To calibrate the spectra in relative flux, the spectrophotometric standard star EG 21 was used. All the data reduction and calibrations were carried out with the standard IRAF procedures. The extracted and flux-calibrated spectrum covers the range ∼4200–7500 Å with a resolution 5.46 ± 0.69 Å, derived from the FWHM of the comparison spectrum lines.

ESO. WR 48a was observed on 2011 April 14 (total integration time of 180 s) using the IR spectrograph and imaging camera SofI (Moorwood, Cuby & Lidman 1998) in long-slit mode on NTT at La Silla Observatory (ESO). The *J*-spectrum scale is 6.96 Å $pixel^{-1}$ that is its resolving power is $R \sim 1000$. The spectral resolution is 13.92 Å (FWHM). Bright stars of spectral type G were observed as a measure of the atmospheric absorption. The spectra were reduced using the standard IRAF procedures: correction for the bad pixels, bias level and sky emission lines subtraction, flat fielding, spectrum extraction, wavelength calibration and telluric correction (for more details see Chené et al. 2012). Unfortunately, no flux calibration was possible and this is why the *J* spectrum was normalized to the stellar continuum (Fig. 3) and used for spectral line analysis only.

AAT. We downloaded from the AAT archive two spectra of WR 48a (the same ones used by Williams et al. 2012) obtained with the RGO spectrograph on 1993 June 21. The spectra were

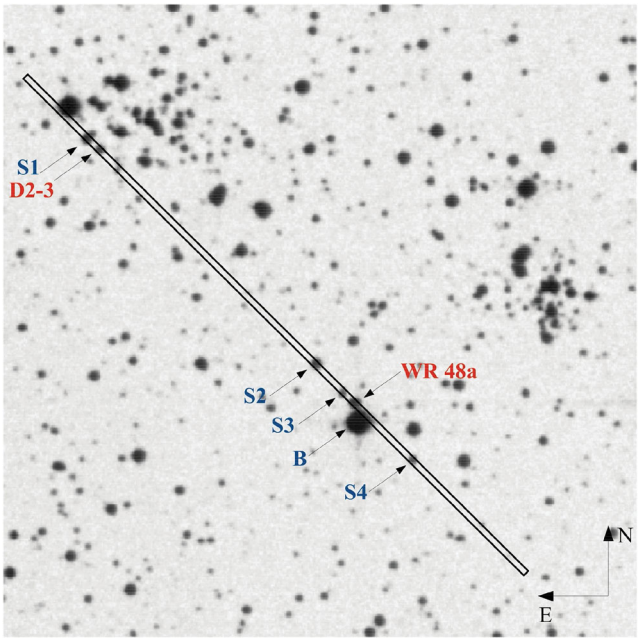

Figure 1. A 5 × 5 $arcmin^2$ field in the vicinity of WR 48a from the MAMA.R.ESO image. The rectangle represents the RSS slit position on the sky. The objects, whose spectra were used in this study, are marked by arrows: WR 48a, D2-3 and several additional stars B, S1, S2, S3 and S4 (see the text for details).

[1] IRAF is distributed by the National Optical Astronomy Observatories, which are operated by the Association of Universities for Research in Astronomy, Inc., under cooperative agreement with the National Science Foundation.

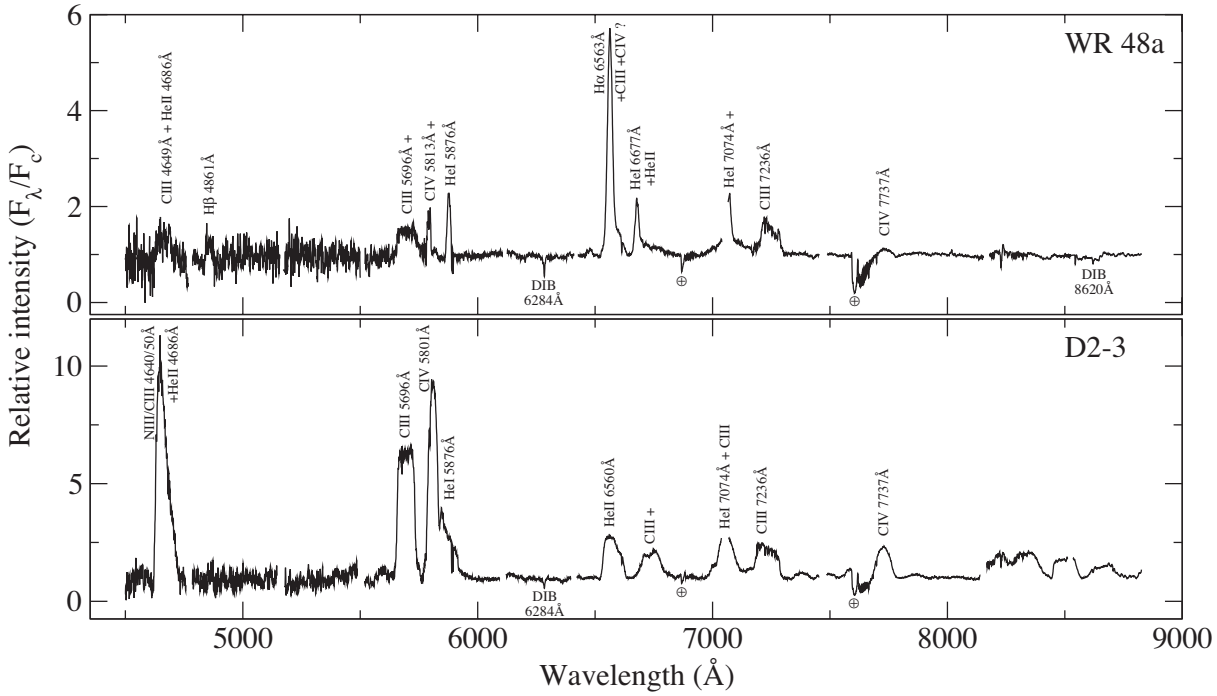

Figure 2. Normalized to the local continuum SALT spectra of WR 48a (upper panel) and D2-3 (lower panel). The gaps in the spectra reflect the RSS interchip gaps. The line identification is based on Williams et al. (2012) and on Mauerhan, Van Dyk & Morris (2009) for WR 48a and D2-3, respectively. The strongest atmospheric absorption bands are marked with Earth symbols.

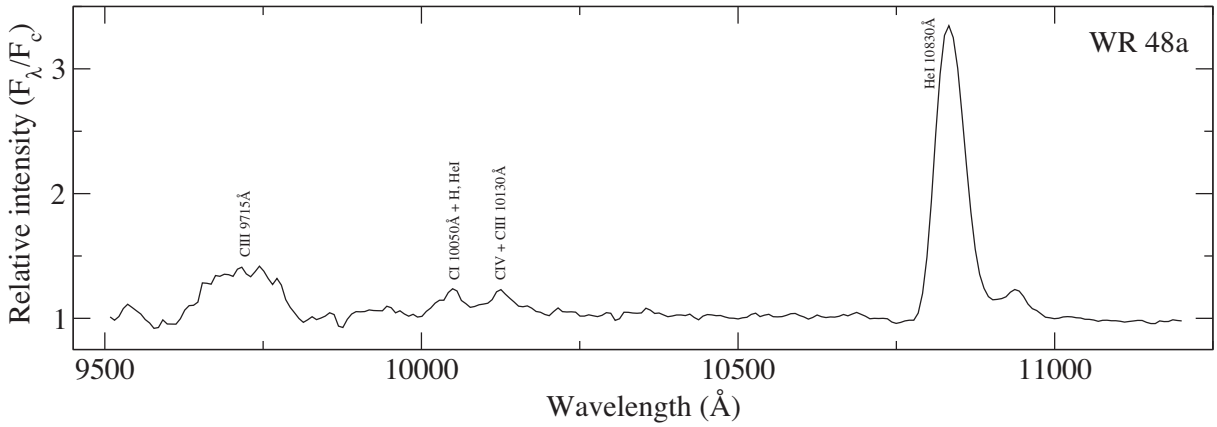

Figure 3. The NTT SofI spectrum of WR 48a normalized to the local continuum. The line identification is based on Williams et al. (2012).

reduced and calibrated by the use of the standard IRAF packages. The spectrophotometric standard star LTT 377, observed during the same night, was used for the relative flux calibration of the spectra. The blue spectrum covers the region from ∼3500 to ∼6700 Å with a resolution 9.65 ± 0.59 Å estimated on the base of the comparison spectrum lines FWHM. The red spectrum covers the region from ∼5300 to ∼11 000 Å and its resolution is 21.5 ± 1.5 Å.

The equivalent widths (EWs) and the FWHM of the strongest emission lines, interstellar absorption lines and diffuse interstellar bands (DIBs), measured in all our spectra are provided in Tables 1–3. The measurements were done with the IRAF tasks SPLOT and SPECTOOL fitting Gaussians to the lines. The error estimates were computed directly in SPLOT and SPECTOOL by running a number of Monte Carlo simulations based on preset instrumental parameters.

2.2 Radio

WR 48a was observed in numerous occasions with the Australia Telescope Compact Array (ATCA) operated by the Australia Telescope National Facility. We have checked the available data in the Australia Telescope Online Archive[2] and made use of the radio observations taken on 2000 February 27 (project code C862; ATCA configuration 6A) and on 2006 December 8 (project code C1610; ATCA configuration 6B). During the project C862, WR 48a was observed at four frequencies 1.4, 2.5, 4.8 and 8.6 GHz with a bandwidth of 128 MHz. However due to data quality, we were able to recover fluxes only at 4.8 and 8.6 GHz. At the two lower

[2] http://atoa.atnf.csiro.au/

Table 1. WR 48a: emission lines.

	SALT (2012 May 27)		AAT blue (1993 June 21)		AAT red (1993 June 21)		ESO NTT (2011 April 14)		SAAO 1.9-m (2103 July 17)	
λ	EW	FWHM	EW	FWHM	EW	FWHM	EW	FWHM	EW	FWHM
C IV 4650			32.18 ± 5.60							
C III 5696	57.71 ± 1.20		70.01 ± 11.0		40.72 ± 1.30					
C IV 5808			48.79 ± 10.8	44.50 ± 12.3	32.07 ± 1.38	49.21 ± 2.13				
				(2244 ± 635)		(2286 ± 110)				
He I 5876	25.20 ± 0.36	14.59 ± 0.23	34.65 ± 6.50	19.14 ± 4.48	20.89 ± 0.98	23.74 ± 1.18				
		(741 ± 12)		(844 ± 229)		(514 ± 60)				
Hα 6563	127.80 ± 0.49	24.56 ± 0.08	70.33 ± 5.91	24.55 ± 2.64	71.55 ± 1.31	29.03 ± 0.59			73.86 ± 1.61	25.66 ± 0.56
		(1121 ± 4)		(1032 ± 121)		(892 ± 27)				(1146 ± 26)
C III+C IV(?) ∼6597	24.23 ± 0.50	42.54 ± 0.93	6.51 ± 6.91	29.62 ± 26.4	5.40 ± 0.94	29.12 ± 5.95				
		(1933 ± 42)		(1273 ± 1201)		(893 ± 271)				
He I 6678	18.14 ± 0.61	17.81 ± 0.46	17.39 ± 6.19	20.75 ± 9.05	13.76 ± 1.77	25.02 ± 2.65			12.04 ± 2.79	15.03 ± 2.40
		(798 ± 21)		(825 ± 407)		(575 ± 119)				(629 ± 108)
He I, C III 7050					21.73 ± 0.87	36.13 ± 1.53			22.44 ± 0.95	
						(1236 ± 65)				
C III, C IV 7230	39.77 ± 0.25				11.39 ± 0.32					
C IV 7737	9.02 ± 0.16	49.61 ± 1.12			10.79 ± 0.89	54.08 ± 5.04				
		(1923 ± 43)				(1924 ± 195)				
C III 9715					91.87 ± 0.72		56.40 ± 0.50			
H, He I, C I 10050					15.44 ± 0.53	49.32 ± 1.84	10.40 ± 0.40			
						(1325 ± 55)				
C III, others 10130					24.42 ± 0.48	43.08 ± 1.02	13.90 ± 0.60			
						(1106 ± 30)				
He I 10830					298.50 ± 0.96	45.09 ± 0.16	132.70 ± 0.60	50.60 ± 0.20		
						(1098 ± 4)		(1348 ± 6)		

Note. Given are the line wavelength (λ) in Å, the line EW in Å, the line FWHM in Å, the FWHM values in units of km s^{-1} are given in parentheses.

Table 2. D2-3: emission lines.

	SALT	
λ	EW	FWHM
C IV 4650	984.10 ± 7.00	
C III 5696	455.30 ± 2.50	
C IV 5808	454.30 ± 32.3	49.24 ± 4.30
		(2542 ± 222)
He I 5876	110.90 ± 7.00	
Hα 6563	144.20 ± 8.40	
C III+C IV(?) ∼6597		
He I 6678	302.60 ± 0.68	
He I, C III 7050		
C III, C IV 7230	108.90 ± 0.47	
C IV 7737	94.84 ± 0.34	59.24 ± 0.23
		(2296 ± 9)

Note. Given are the line wavelength (λ) in Å, the line EW in Å, the line FWHM in Å, the FWHM values in units of km s^{-1} are given in parentheses.

Table 3. Interstellar absorption features.

λ	WR 48a	D2-3
Na I 5889	1.26 ± 0.08	1.37 ± 0.08
Na I 5995	1.22 ± 0.09	1.08 ± 0.07
6283	2.70 ± 0.10	2.82 ± 0.13
6614	0.38 ± 0.03	0.57 ± 0.03
K I 7699	0.50 ± 0.03	0.42 ± 0.03
8620	0.55 ± 0.03	0.56 ± 0.04

Note. Given are the absorption line identification or the DIB wavelength (λ) in Å and its EW in Å for WR 48a and D2-3, respectively.

frequencies, there were a lot of interferences in the data that resulted in unreliable maps. Because of that, we were unable to make any conclusions about the WR 48a radio fluxes at 1.4 and 2.5 GHz. In the project C1610, WR 48a was observed at two frequencies 4.8 and 8.6 GHz with a bandwidth of 128 MHz (Fig. 4). We were able to reduce all data and estimate the WR 48a fluxes at both used radio bands. 1934-638 was used as a primary flux calibrator in both bands but different phase calibrators were chosen: 1251-713 for C862 and 1352-63 for C1610, respectively. The whole data reduction process was carried out using the standard NRAO AIPS[3] procedures. The task IMAGR was used to produce the final total intensity images of WR 48a. Radio fluxes were then measured, by fitting Gaussian model using the AIPS task JMFIT.

2.3 X-rays

To broaden the study of the X-ray properties of WR 48a, especially, that on its long-term X-ray variability, we have checked the archives of the modern X-ray observatories (e.g. *Chandra*, *XMM–Newton*, *ROSAT*, *Swift*). Thus, in addition to the already analysed and published data (see Zhekov et al. 2011, 2014), we found two *ROSAT* and 33 pointed *Swift* observations. We also gave some consideration to the *Chandra* ACIS-I data on WR 48a which are heavily piled up and thus cannot be used for spectral analysis.

[3] www.aips.nrao.edu/index.shtml

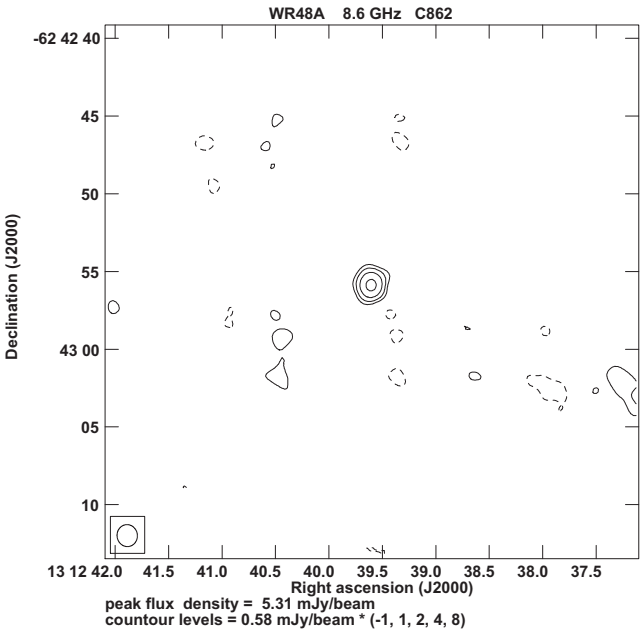

Figure 4. Radio map of WR 48a at 8.6 GHz based on data from the ATCA project C862. The first contour in map represents 3σ detection limit.

Swift. WR 48a was observed multiple times between 2010 December 15 and 2013 February 27 with typical exposure time of 2400–5000 s. From all the 33 pointed observations (ObsID from 00031900001 to 00031900033), one (ObsID 00031900017) was not included in this analysis due to its very short exposure time (∼70 s). Following the Swift XRT Data Reduction Guide,[4] we extracted the source and background spectra for each observation. Extraction regions had the same shape and size for each data set (see Fig. 5). For our analysis, we used the response matrix (swxpc0to12s6_20010101v014.rmf) provided by the most recent (2014 February 02) *Swift* calibration files[5] and we also used the package XRTMKARF to construct the ancillary response file for each data set.

ROSAT. WR 48a fell in the *ROSAT* field of view in two occasions in 1997 February. The corresponding PSPC data sets are rp190020n00 (February 5; 20.5 arcmin off-axis; exposure time 740 s) and rp190249n00 (February 23; 34.3 arcmin off-axis; exposure time 1080 s). Following the recommendations for the *ROSAT* Data Processing,[6] we extracted the source and background spectra (see Fig. 5). Since the data were taken after 1991 October 14, we adopted the response matrix pspcb_gain2_256.rmf and we used the package PCARF to construct the ancillary response file for each observation. Because of the limited photon statistics of the *ROSAT* spectra of WR 48a (each has no more than 50 source counts), we combined them and used the resultant spectrum in our analysis (see Section 3.5).

Chandra. WR 48a was detected by *Chandra* (ObsID: 8922) but the pile up in the ACIS CCD is very high (see footnote 5 in Zhekov et al. 2011). Nevertheless, we used the Chandra Interactive Analysis of Observations 4.4.1[7] data analysis software to formally extract an

[4] http://swift.gsfc.nasa.gov/analysis/xrt_swguide_v1_2.pdf
[5] http://heasarc.gsfc.nasa.gov/docs/heasarc/caldb/swift/
[6] http://heasarc.gsfc.nasa.gov/docs/rosat/rhp_proc_analysis.html
[7] For details, see http://cxc.harvard.edu/ciao/

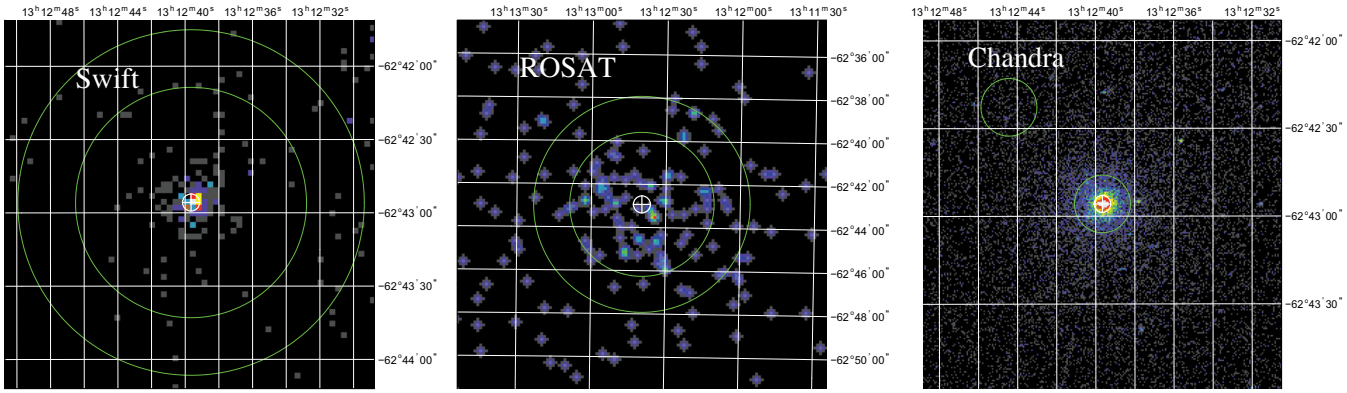

Figure 5. Raw *Swift* (ObsId: 00031900028), *ROSAT* (ObsId: rp190249n00) and *Chandra* ACIS-I (ObsId: 8922) images. RA (J2000) and Dec. (J2000) are on the horizontal and vertical axes, respectively. The circled plus sign denotes the optical position of WR 48a (SIMBAD). The inner circle marks the source extraction region. For the *Swift* and *ROSAT*, the annulus denotes the background extraction region while the background region is another circle (upper left from the image centre) for the case of *Chandra* ACIS-I.

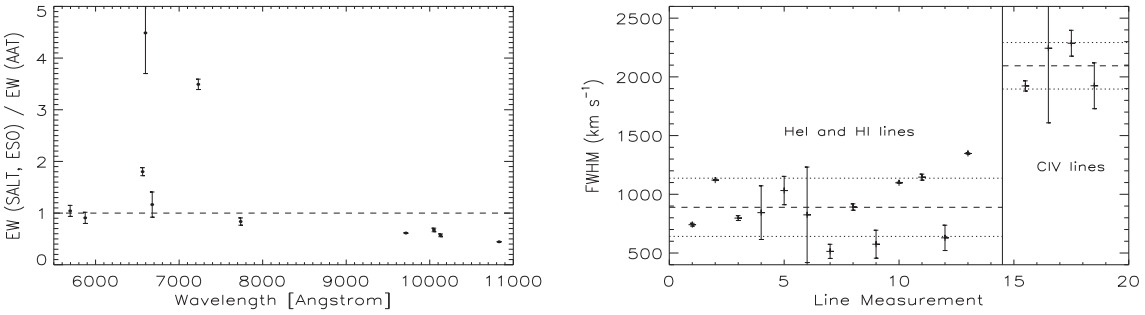

Figure 6. The WR 48a line parameters. Left-hand panel: the ratio of EWs of various emission lines in the optical and NIR spectra of WR 48a: EW(SALT)/EW(AAT) for $\lambda < 8000$ Å; EW(ESO)/EW(AAT) for $\lambda > 9000$ Å. Right-hand panel: the FWHM of He I 5876, 6678, 10830 Å and Hα (line measurement <14); C IV 5808 and 7737 Å (line measurement >15). The term 'line measurement' (*X*-axis) has no specific meaning and is used only for counting the derived FWHM values.

X-ray source spectrum and the background emission in the source vicinity (see Fig. 5). We could thus estimate the source background-subtracted count rate. Despite being affected by the strong pile up, we made some use of this parameter in the discussion of the X-ray light curve of WR 48a (see Section 3.5).

For the spectral simulations in this study, we made use of version 11.3.2 of XSPEC (Arnaud 1996).

3 RESULTS

3.1 Spectral lines

For WR 48a and D2-3, we measured the EW and the FWHM for all the spectral lines that were detected in the optical and NIR spectra at hand: SALT, AAT blue and red channels, ESO NTT, SAAO 1.9-m telescopes. Before estimating the FWHM values in units of km s^{-1}, we corrected them for the instrumental broadening: $\mathrm{FWHM}_0 = \sqrt{\mathrm{FWHM}^2 - \mathrm{FWHM}^2_{\mathrm{sp.res.}}}$ ($\mathrm{FWHM}_{\mathrm{sp.res.}}$ is the spectral resolution for the given spectrum, see Section 2.1).

The corresponding results for WR 48a are given in Table 1. Since the EWs do not depend on the spectral resolution, their values can give an indication for spectral changes. The EW ratios from the WR 48a spectra over a time difference of about 20 yr are shown in Fig. 6. We see that there is some indication that spectral lines (especially, hydrogen–helium lines) in the optical are stronger in 2012 (the SALT observation), while the spectral lines in the NIR were stronger in 1993 (the AAT observation). The latter is likely due to appearance of some strong continuum in the NIR, probably a dust emission in 2012.

It is interesting to note that the FWHM values of the optical–NIR emission lines in WR 48a give some indication for a possible presence of two gas flows different in kinematic sense. Namely, we see that all the 'cool' lines (He I and H I lines) are considerably narrower than those of high-excitation ionic species (e.g. C IV). Fig. 6 (right-hand panel) is an illustration of this difference. We note that the C IV lines in WR 48a are as broad as in the WC8 star D2-3 (Table 2). Then, could it be that these 'hot' lines belong to the WC8 star in WR 48a while the narrower helium–hydrogen lines (the 'cool' lines) belong to its companion star? We will return to this issue in Section 3.3.2.

3.2 Interstellar absorption features

For WR 48a and D2-3, we measured the EWs of all the identified interstellar absorption lines and diffuse interstellar bands in the SALT data. We just recall that the spectra of these two objects were obtained simultaneously. The results are given in Table 3. We see that the EWs of the interstellar absorption features are practically the same for both objects. This indicates that WR 48a and D2-3 are located at the same distance from us. Keeping in mind that D2-3 is

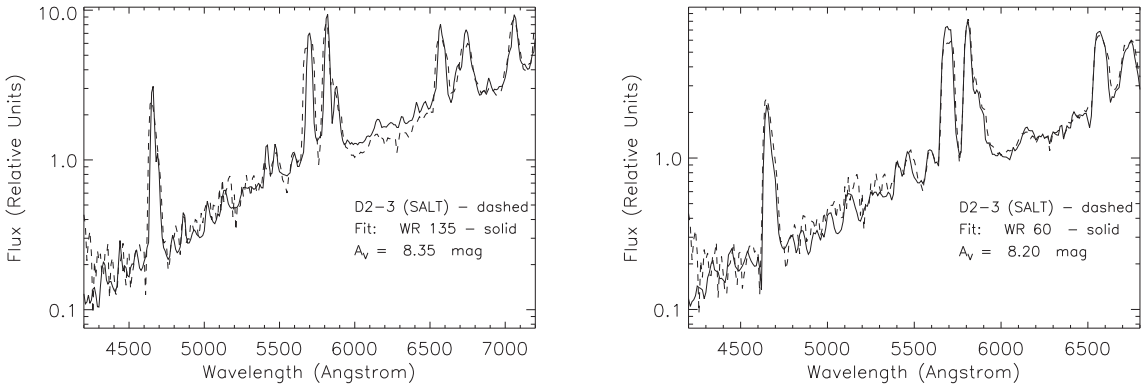

Figure 7. Fits to the SALT spectrum of D2-3. The 'theoretical' spectra are those of WR 135 and WR 60 (both are WR stars of the WC8 type). The bin size is 10 Å.

a member of Danks 2, one of the two central clusters in the G305 star-forming complex (Davies et al. 2012), we obtain an important confirmation that WR 48a is located at the distance of ∼4 kpc to Danks 1 and 2 (e.g. Danks et al. 1983; Davies et al. 2012). This conclusion is supported by the fact that 'identical' EWs values are measured for a near-by star S1 (D2-7) – another member of the open cluster Danks 2 (see Appendix A).

3.3 Global spectral fits

All the spectral fits were done by making use of the Levenberg–Marquardt method for non-linear fitting (e.g. section 15.5 in Press et al. 1992). As theoretical spectra, we used the observed flux-calibrated spectra of stars of different spectral types taken from the spectral libraries (on-line data in SIMBAD) or from the archives of various observatories. In the spectral fits, the interstellar medium (ISM) extinction was also taken into account by making use of the standard ISM extinction curve of Fitzpatrick (1999).

3.3.1 Spectral fits to D2-3

Since D2-3 (2MASS J13125770−6240599; WR48-2[8]) was classified WR star of the WC8 spectral type (Mauerhan et al. 2009; Davies et al. 2012), we fitted its SALT spectrum with spectra of classical WC8 stars and taking into account the interstellar extinction. Namely, we used the spectra of WR 135 (3140–7221 Å) and WR 60 (3384–6867 Å) from the atlas of WC star spectra by Torres & Massey (1987). Since these spectra are not corrected for the interstellar extinction, we first dereddened them with $E(b-v) = 0.34$ mag and $E(b-v) = 1.40$ mag for the WR 135 and WR 60, respectively ($E(B-V) = 1.21E(b-v)$, see section 8.2 and table 28 in van der Hucht 2001). We rebinned the observed spectrum to increase its signal-to-noise (S/N) ratio and we rebinned the theoretical spectra correspondingly as well. We explored a rebinning of 2, 5 and 10 Å to check how the fit results depend on this parameter. We recall that the SALT spectra were flux calibrated but in relative units (see Section 2.1) thus the free parameters in the fits were the scaling factor for the theoretical spectrum at some fiducial wavelength and the optical extinction to D2-3. We note that in the case under consideration the spectral scaling factor has no direct physical meaning. On the other hand, such fits allow us to derive an estimate of the optical extinction and, as expected and also proved in the fits, its derived value does not depend on what wavelength the scaling parameter was defined at.

Fig. 7 presents some results from our fits. We see that the theoretical WC8 spectra nicely match the SALT spectrum of D2-3 which confirms its spectral classification as a WC8 WR star. The derived optical extinction to this object is $E(B-V) = 2.67 \pm 0.03$ mag (the uncertainty corresponds to the variance of the mean of the values derived in the fits for different spectral rebinning) or $A_V = 8.28 \pm 0.09$ mag ($A_V = 3.1E(B-V)$). We note that the extinction to D2-3 is consistent with the value we derived for another member of the open cluster Danks 2, S1 (D2-7): $E(B-V) = 2.73$ mag (see Appendix A).

3.3.2 Spectral fits to WR 48a

WR 48a was classified as WR star of the WC8 type (van der Hucht 2001). It has been suggested that WR 48a is a binary star and the relatively weak spectral lines in its spectrum hint on a presence of an additional source of continuum emission that is attributed to the companion star in the system. Williams et al. (2012) gave arguments for the companion to be an emission-line star, O5Ve. To explore this possibility in some detail, we carried out two-component spectral fits to the SALT and AAT spectra of WR 48a that take into account the interstellar extinction. We note that for these fits we constructed one common AAT spectrum. Namely, we adopted the AAT blue-channel spectrum for wavelengths shorter than 5000 Å and the AAT red-channel spectrum otherwise. The details of the fitting procedure are as follows.

For the first component of the spectral fit, we chose the SALT spectrum of the D2-3 which allowed us to explore a larger spectral range (the SALT spectrum of D2-3 spans in wavelength almost to 9000 Å while that of WR 135 from the Torres & Massey atlas spans only to 7200 Å). This spectral component was dereddened by $E(B-V) = 2.67$ mag to derive the 'theoretical' spectrum of the first component in the fit. For the second component in the WR 48a fit, we used spectra from STELIB library (Le Borgne et al. 2003) or from the archives of various observatories. We recall that all the 'theoretical' spectra were flux calibrated. The free parameters in the fit were the scaling factor for each spectral component and the interstellar extinction (both components were subject to common interstellar extinction). Thus the spectral fits of the SALT and AAT spectra of WR 48a provided us with an estimate of the interstellar extinction to this object and of the relative brightness of the stellar

[8] Galactic Wolf Rayet Catalogue; http://pacrowther.staff.shef.ac.uk/WRcat/index.php

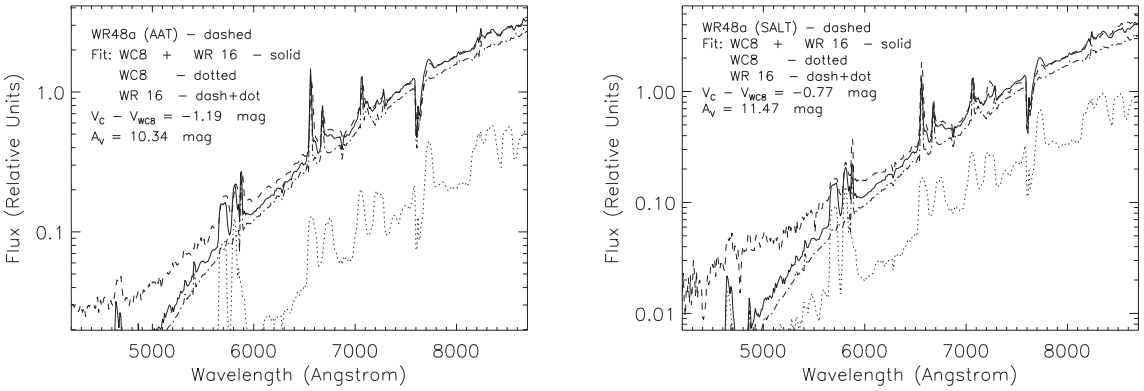

Figure 8. Two-component fits to the AAT and SALT spectra of WR 48a. The first component is the SALT spectrum of the D2-3 star, and the second component is the spectrum of WR 16 (a WR star of the WN8h type). The bin size is 10 Å.

components. We represented the latter by the difference of the intrinsic V magnitude of the WC8 star (V_{WC8}) and its companion star (V_C): $\Delta V = V_C - V_{WC8}$.

Since no spectral information is available about the presumable stellar companion of the WC8 star in WR 48a, we explored a range of spectral types for it. For this, we made use of spectra from the STELIB library (Le Borgne et al. 2003) and data from the European Southern Observatory (ESO) archives. We ran global two-component fits to the SALT and AAT spectra of WR 48a with spectra of WR, luminous blue variable (LBV), O, B and A stars for the second component. We note that in these fits matching the observed WC8 spectral features in the WR 48a spectra was not a problem: these spectral lines are matched well if they are scaled appropriately by the continuum of the second stellar component. The basic challenge in these fits was to match the spectral lines of helium and hydrogen (He I 5876, 6678 Å, Hα 6563 Å). Our best fit with this respect was that with a spectrum of a WR star of late WN type (WR 16; van der Hucht 2001) for the second spectral component. Fig. 8 presents the results from this two-component (WC8+WN8h) fit. The spectral fits with LBV, O, B or A-star spectrum for the second component did not give a good match to the helium and hydrogen lines (see Appendix B). A few things are worth noting.

In overall, the interstellar extinction towards WR 48a in the V filter is higher by 2–3 mag than that towards the near-by WC8 star D2-3. In all the fits, the WR 48a spectra at shorter wavelengths ($\lambda < 5500$ Å) were not matched well by the two-component fit. We tried to improve the quality of the fit by adding another component (e.g. a blackbody or a power-law emission) but we could not succeed. We note that the quality of the SALT and AAT spectra in that spectral range is not very good and this might be the reason for such a discrepancy. We thus think that new spectra with much better sensitivity are needed to resolve this issue. In the AAT spectrum, the companion star is about three times brighter than the WC8 component ($\Delta V = V_C - V_{WC8} = -1.19$ mag). This is consistent with the estimate by Williams et al. (2012) based on the ratio of the 5696 and 5813 Å lines in the AAT spectra of WR 48a and of the WC8 standard WR 135. Some spectral changes have taken place in the optical over a period of time of about 19 yr, that is between 1993 June (AAT) and 2012 May (SALT): (a) the relative brightness of the companion decreased; (b) the interstellar (or circumstellar) extinction towards WR 48a increased. We will further discuss these results in Section 4.

3.4 Radio properties

As discussed in Section 2.2, we were able to derive the radio fluxes of WR 48a from the observations analysed in this study. The results are given in Table 4. Although of limited spectral coverage (observed fluxes only at two frequencies), these results indicate that the radio source in WR 48a is likely of thermal origin: $F_\nu \propto \nu^\alpha, \alpha > 0$. In fact, the derived power-law index (see Table 4) is within (1–2)σ from the canonical spectral index of $\alpha = 0.6$ for the thermal radio emission from the stellar wind in massive stars (Panagia & Felli 1975; Wright & Barlow 1975). We recall that in their analysis of the radio data on the G305 star-forming region, Hindson et al. (2012) also reported a detection of a thermal radio source ($\alpha = 0.6$) associated with WR 48a. Comparing the radio fluxes from all these observations, two things seem conclusive: (a) some variability in the radio emission of WR 48a is present; (b) the radio emission of WR 48a is very likely of thermal origin.

For the case of thermal radio emission, we can estimate the ionized mass-loss rate for an assumed constant velocity smooth (no clumps) wind using the result of Wright & Barlow (1975): $\dot{M} = C_0 v_\infty S_\nu^{0.75} d_{\rm kpc}^{1.5}$ M$_\odot$ yr^{-1}, where $C_0 = 0.095\mu/[Z(\gamma g \nu)^{1/2}]$. Here v_∞ is the terminal wind velocity in km s^{-1}, S_ν is the radio flux in Jy at frequency ν in Hz, $d_{\rm kpc}$ is the stellar distance in kpc, μ is the mean atomic weight per nucleon, Z is the rms ionic charge, γ is the mean number of free electrons per nucleon and g is the free–free Gaunt factor (see equation 8 in Abbott et al. 1986 for a suitable approximation of the Gaunt factor). Since WR 48a is a WC8 WR star, we adopt $Z = 1.4$, $\gamma = 1.3$, $\mu = 7.7$ typical for such an object (van der Hucht, Cassinelli & Williams 1986), $v_\infty = 1700$ km s^{-1} (the mean wind velocity for WC8 stars, see table 27 in van der Hucht 2001) and $d_{\rm kpc} = 4$ (see Section 3.2). So, the derived radio fluxes correspond to a mass-loss rate of $\dot{M} = (3.7\text{–}6.4) \times 10^{-4}$ M$_\odot$ yr^{-1}. We only note that the WR 48a radio fluxes of 2.4 mJy (5.5 GHz) and 2.9 mJy (8.8 GHz) from Hindson et al. (2012) correspond to a

Table 4. WR 48a: radio fluxes.

Date	4.8 GHz	8.64 GHz	α
2000 Feb 27	3.94 ± 0.21	5.39 ± 0.46	0.53 ± 0.17
2006 Dec 8	1.90 ± 0.27	3.64 ± 0.18	1.10 ± 0.25

Note. Given are the date of radio observation, the radio fluxes with the 1σ error in mJy and the spectral index ($F_\nu \propto \nu^\alpha$).

mass-loss rate of $\dot{M} = (3.9\text{-}4.1) \times 10^{-4}\ M_{\odot}\ yr^{-1}$. We thus see that the level of thermal radio emission from WR 48a suggests that this WC8 star has a very massive stellar wind.

3.5 X-ray light curve

As reported by Zhekov et al. (2014), WR 48a is a variable X-ray source on a time-scale of a few years. The *Swift* observations, taken on a quasi-monthly basis over a more than 2-yr period of time, provide additional information in this respect. We extracted source and background spectra for 32 *Swift* observations. Unfortunately, the short exposure time (see Section 2.3) and the decreased X-ray emission from WR 48a do not allow for carrying out a spectral analysis in detail. On the other hand, we used the data to construct an X-ray light curve. For comparison, we converted the *XMM–Newton* and *Chandra* fluxes into the *Swift* reference system. This was done in the following manner.

For each of the *XMM–Newton* and *Chandra*-HETG observations, we simulated a *Swift* spectrum in XSPEC by making use of the *Swift* response matrix and the ancillary response files adopted in our study (see Section 2.3). This provided the corresponding count rate in the *Swift* reference system. We examined all the ancillary response files of the *Swift* observations and found that the telescope effective area has not changed considerably (e.g. by no more than a few per cent) over the 2-yr monitoring of WR 48a. We thus used the ancillary response file for the *Swift* observation (ObsID: 00031900028), taken only 2 d before the *Chandra*-HETG observation, in all the simulations of this kind. Also, the best-fitting two-shock models that correspondingly matched the *XMM–Newton* and *Chandra*-HETG spectra (see Zhekov et al. 2011, 2014) were used in the XSPEC simulations.

As to the *Chandra*-ACIS-I observation, we recall that it is heavily piled up (see Section 2.3) and we made use of the *Chandra* count rate prediction tool PIMMS[9] to get an estimate of the flux level of WR 48a. Namely, we adopted an absorbed two-temperature thin-plasma model (model APEC in XSPEC) and fitted the X-ray spectrum of WR 48a from the *XMM–Newton* observation in 2008 January. We then ran a series of PIMMS simulations adopting the *Chandra*-ACIS-I parameters for the AO8 observation period when the data were actually obtained. In these simulations, the observed flux was scaled while the shape of the spectrum was the same (i.e. no change of the plasma temperature and the X-ray absorption). We note that PIMMS estimates the amount of pile up in the data and thus provides a pile up-corrected count rate representative of its observed value. Fig. 9 presents the results from our PIMMS simulations. A comparison with the observed count rate in *Chandra*-ACIS-I data illustrates that the X-ray flux of WR 48a in 2008 December was at least as high as it was in 2008 January (the *XMM–Newton* observation). For the X-ray light curve, we then assumed a value of the *Chandra*-ACIS-I flux equal to that in the *XMM–Newton* observation.

Fig. 10 presents the background-subtracted light curve of WR 48a 'expanded' with the *XMM–Newton* and *Chandra* data points. We note a very good correspondence between the fluxes (count rates) from the *Chandra* -HETG observation on 2012 October 12 and the *Swift* observation on 2012 October 10. This in turn means that the point-to-point fluctuations in the *Swift* light curve of WR 48a might be real and not an instrumental artefact.

[9] Portable, Interactive Multi-Mission Simulator; http://asc.harvard.edu/toolkit/pimms.jsp

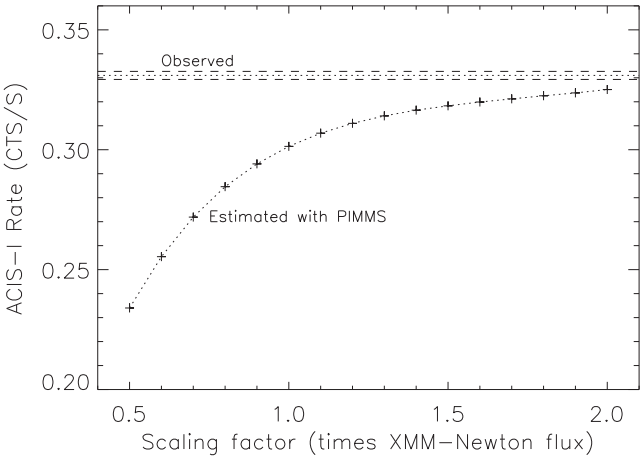

Figure 9. The *Chandra*-ACIS-I count rates from the PIMMS simulations of the X-ray emission of WR 48a. The count rates are corrected for the pile up. The two dashed lines bracket the 1σ confidence interval of the observed count rate of WR 48a (*Chandra* ObsID: 8922).

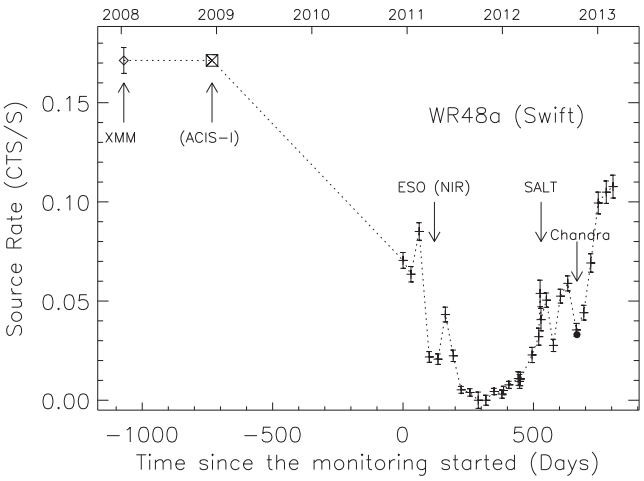

Figure 10. The *Swift* X-ray (0.5–10 keV) light curve of WR 48a. Given on the axes are: the time since the *Swift* monitoring started in 2010 December (*X*-axis; the calendar year of observations is shown on the upper *X*-axis) and the background-subtracted count rate (*Y*-axis). For comparison, the data points for the *XMM–Newton* (2008 January), *Chandra* ACIS-I (2008 December) and *Chandra* HETG (2012 October) observations converted into *Swift* count rates (see text) are labelled 'XMM' (diamond), '(ACIS-I)' (crossed square) and 'Chandra' (filled circle), respectively. The ESO (NIR) and the SALT observation dates are marked as well.

Finally, it is interesting to check the level of X-ray emission from WR 48a on even a longer time-scale by considering the *ROSAT* observations carried out in 1997 February. To do so, we used the two-shock model that perfectly matched the X-ray emission from WR 48a as of 2008 January (the *XMM–Newton* observation; Zhekov et al. 2011). Fig. 11 shows the total *ROSAT* spectrum overlaid with the two-shock model for the *XMM–Newton* observation. We see that the *ROSAT* data are consistent with this model which also means that the X-ray emission of WR 48a in 1997 February was about the same as of 2008 January (the *XMM–Newton* observation). In fact, if we kept the spectral shape unchanged (i.e. plasma temperature and X-ray absorption fixed) and varied only the normalization parameter of the model, the best-fitting *ROSAT* flux was about 70 per cent of

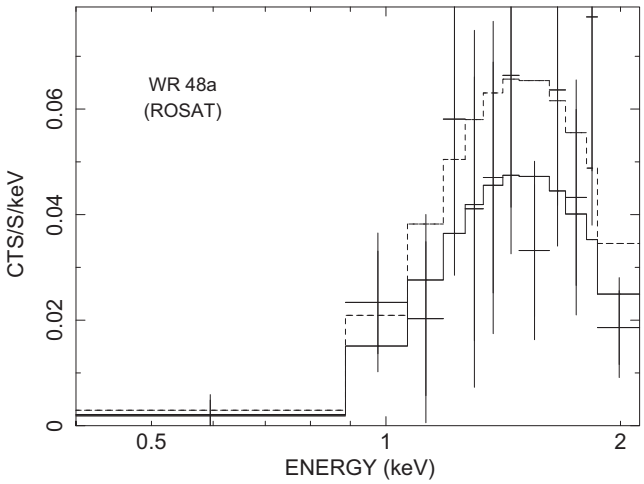

Figure 11. The background-subtracted *ROSAT* spectrum of WR 48a rebinned to have a minimum of 10 counts bin^{-1}. Overlaid are: (a) the two-shock model that perfectly fits the 2008 January *XMM–Newton* spectra of WR 48a (Zhekov et al. 2011) – dashed line; (b) the same model but with varied normalization parameter to match the flux level of the *ROSAT* spectrum (see text) – solid line.

that in the *XMM–Newton* data but the difference is within the 1σ confidence interval for the *ROSAT* flux.

Thus from the X-ray light curve of WR 48a, we have indications of a high and stable X-ray flux for a period of 10 yr or so (from the *ROSAT*, 1997 February, through the *XMM–Newton*, 2008 January, to the *Chandra*-ACIS-I, 2008 December, observation). Also, we see that recently the X-ray emission from WR 48a decreased to a much lower level over a period of 1–2 yr (2010 December–2013 February). In Section 4, we will discuss some implications from such a long-term X-ray variability in WR 48a.

4 DISCUSSION

The basic results from our analysis of the new (optical and NIR) and archive (optical, radio, X-rays) data on the dusty WR star WR 48a are as follows.

In the optical, the spectrum of WR 48a is acceptably well represented by a sum of two spectra: of a WR star of the WC8 type and of a WR star of the WN8h type. An indication for a presence of two different gas flows (stellar winds) is also found from the quite different widths of the emission lines of 'cool' species (He I and H I) and of 'hot' species (C IV): ∼900 versus ∼2100 km s^{-1}, respectively. Some variability of the optical emission of WR 48a is established from the comparison of the optical spectra of WR 48a obtained in 2011–2012 and in 1993. This is indicated by the change of the EWs of some emission lines, the relative brightness of the WC8 and WN8h spectral components and the optical extinction to this object.

In the radio, WR 48a is very likely a thermal source and also shows some variability on a time-scale of a few years or so. The level of the radio emission suggests a relatively high mass-loss rate of this dusty WR star ($\dot{M} \approx$ a few $\times\ 10^{-4}$ M$_\odot$ yr^{-1}).

In the X-rays, WR 48a is known to be a variable source on a time-scale of a few years (Zhekov et al. 2014) and its variability on a shorter time-scale (within 1–3 yr) is now established as well.

We recall that WR 48a shows recurrent dust formation on a 30-yr time-scale which suggests that it is a long-period colliding wind binary (Williams et al. 2012). The importance of CSWs for the physics of this object is also supported by its high X-ray luminosity (Zhekov et al. 2011) and by the fact that the forbidden line of Si XIII in its X-ray spectrum is strong and not suppressed (Zhekov et al. 2014). The latter indicates that a rarefied 10–30 MK plasma forms far from strong sources of ultraviolet emission, most likely in CSWs in a wide binary system. It is thus interesting to 'project' our results on to this physical picture and see what new they could add or help us constrain in it.

The basic features of CSWs in episodic dust makers are best illustrated by the prototype for these objects, the WR+O binary WR 140. The maximum of the NIR emission, and the sudden onset of dust formation, occurs at or immediately after the orbital phase corresponding to the periastron passage (Williams et al. 1990). The X-ray emission from WR 140 is strong and variable (Williams et al. 1990; Zhekov & Skinner 2000; Pollock et al. 2005). The non-thermal radio emission of this system is strong and variable (Williams et al. 1990; White & Becker 1995; Dougherty et al. 2005). All these characteristics are result from CSWs in a wide binary system with highly elliptical orbit (Williams et al. 1990).

Apart from the NIR variability, the X-ray properties of WR 48a play a key role for the presumable CSW picture in this object. In fact, WR 48a is the X-ray most luminous WR star in the Galaxy after the black hole candidate Cyg X-3, *provided it is physically associated with the open clusters Danks 1 and Danks 2 at a distance of* d ∼ *4 kpc* (Zhekov et al. 2011). We now have a good argument that this is indeed the case. Our analysis of the SALT spectra of WR 48a and the nearby WR star D2-3, which is a member of Danks 2 (e.g. Davies et al. 2012), showed that both objects are located at about the same distance from us (see Section 3.2). Thus, the very high X-ray luminosity of WR 48a presents a solid support for the CSW picture in this object.

However, we have to keep in mind that there are some important observational findings that pose problems for the standard CSW paradigm in the case of WR 48a.

As noted by Williams et al. (2012), the IR light curve of WR 48a differs appreciably from that of canonical dust makers as WR 140. Namely, the IR emission of the latter surges to a maximum in a short period of time (due to the sudden onset of dust formation) and then decreases much more slowly to its minimum (see fig. 2 in Williams et al. 1990). Opposite to this, the IR light curve of WR 48a gradually changes between its minimum and maximum values (see fig. 3 in Williams et al. 2012) and even shows some 'mini eruptions' as observed in another episodic dust maker WR 137 (Williams et al. 2001).

On the other hand, the sudden onset of dust formation is associated with the periastron passage in a wide binary system with elliptical orbit (Williams et al. 1990). This means that the maximum of the IR emission occurs near the orbital phase of the minimum binary separation. Interestingly, the *Chandra*-HETG X-ray observation of WR 48a was carried out near the maximum of the IR emission of this dusty WR star. The analysis of these data *along the lines of the adiabatic CSW picture (appropriate for wide WR binaries)* showed that the binary separation at the moment of the *Chandra* observation (2012 October 12) was *larger* than that at the moment of the *XMM–Newton* observation (2008 January 9) of WR 48a which was taken approximately 5 yr earlier (Zhekov et al. 2014). Thus, the maximum of the IR emission from WR 48a does not seem to be related to the minimum binary separation (the periastron passage) in this presumable wide binary system. It may well be that the mechanism for IR emission in WR 48a is different from that in canonical dust makers as WR 140.

Since WR 48a is very likely a thermal radio source (see Section 3.4), the lack of non-thermal radio (NTR) emission from this object is another atypical characteristic of a possible wide CSW binary. We recall that in general the CSW binaries are NTR sources (Dougherty & Williams 2000). We could think of at least two possible reasons for such a discrepancy.

First, the NTR source could be heavily absorbed by the massive wind(s) in the binary if it were located deep in the radio photosphere. We note that for the typical WC abundances the mass-loss rate of the stellar wind(s) in WR 48a is very high $\dot{M} = (3.7–6.4) \times 10^{-4}\,M_{\odot}\,yr^{-1}$ (see Section 3.4). It is very high even if we assume the typical WN abundances (van der Hucht et al. 1986) or the solar abundances (Anders & Grevesse 1989) for the stellar wind(s): $\dot{M} = (3.0–5.2) \times 10^{-4}\,M_{\odot}\,yr^{-1}$ (WN); $\dot{M} = (1.0–1.7) \times 10^{-4}\,M_{\odot}\,yr^{-1}$ (solar). For these values of the mass-loss rate and using equation (11) from Wright & Barlow (1975), we derive that the radius of the radio photosphere (defined for a radial optical depth from infinity of 0.244) is in the range 95–203 au for the radio frequencies of the WR 48a observations. In turn, the radius of the radial optical depth of unity is 23–50 au. Thus, if the NTR source in WR 48a is located in the stellar wind deeper than that radius, we may have missed its detection.

Second, could it be that *no* NTR source is physically present in WR 48a? In general, we need two ingredients for generating non-thermal radio emission: relativistic electrons and a magnetic field. The relativistic electrons are assumed to be born in strong shocks through the mechanism of diffusive shock acceleration. This mechanism also requires a presence of a magnetic field (e.g. Bell 1978). Strong shocks are definitely present in a colliding wind binary but if there is no magnetic field in WR 48a, then the generation of NTR emission would not be possible. If future, multifrequency, radio observations establish with certainty that WR 48a has no *intrinsic* NTR emission, this will be a very important finding. We note that the spectral fits to the optical emission of WR 48a indicated that its binary components are evolved stars, namely, a WC and a WN (or a LBV) star (see Section 3.3.2). Thus, the lack of NTR emission will be a sign that no magnetic field is present in such an evolutionary phase of massive stars. This will also mean that in all the WR+O binaries that are source of NTR emission the O star provides the magnetic field that is needed for the relativistic electron production in strong shocks.

Thus, we see that although there are observational facts that strongly indicate the presence of colliding stellar winds in WR 48a, there is also a number of observational facts which indicate that the physical picture in this dusty WC star might be more complex than that.

Along these lines, we mention the relative variability between the WC and the WN components as revealed by the change of the EWs of some strong optical lines and by the spectral fits to the optical emission of WR 48a (see Sections 3.1 and 3.3.2). This spectral variability is also accompanied by a change in the optical extinction to this object (see Section 3.3.2). We believe that this variable optical extinction is of local origin. More specifically, we mean the additional extinction to WR 48a compared to that to D2-3 (the near-by member of the open cluster Danks 2): the A_V value for the former is by 2–3 mag higher than for the latter. Interestingly, the higher local extinction is observed near the maximum of the IR emission from WR 48a (see fig. 3 in Williams et al. 2012): the SALT spectrum (2012 May 27) shows higher optical extinction than the AAT spectra (1993 June 21). The local dust formation, with a variable rate of dust production, is a possible mechanism that could explain these results. Then, the origin of the dust in WR 48a is a key issue: does the circumstellar dust form in CSWs in a wide binary with elliptical orbit or in a different place?

We already discussed some observational findings that strongly support the standard CSW picture in WR 48a and some that pose problems for its validity. In this respect, we recall that the highest rate of dust formation in CSWs (maximum IR emission) is associated with the periastron passage (minimum binary separation) in a wide binary with elliptical orbit. However, the analysis of the X-ray data of WR 48a, obtained with *Chandra* near the maximum of the IR emission, showed that the binary separation was not near its minimum value (Zhekov et al. 2014). Thus, could it be that the dust formation is related to some LBV-like activity, as the latter might be indicated by the relative variability between the WC and the WN components in the optical spectrum of WR 48a? Could WR 48a be similar to the binary (or triple) system HD 5980 in the Small Magellanic Cloud having a LBV object as one of its component and showing a 40-yr variability cycle (see Koenigsberger et al. 2010 and the references therein)? We only note that dust exists in the LBV environment (e.g. McGregor, Hyland & Hillier 1988) and the presence of a WC star (a carbon-rich object) in WR 48a may additionally facilitate the dust production in this system.

The high mass-loss values, deduced from the analysis of the radio data, hint on something unusual in the dusty WR star WR 48a. Similar indication comes also from the X-ray light curve obtained with *Swift* and supplemented by data from *Chandra*, *ROSAT* and *XMM–Newton* (see Section 3.5 and Fig. 10). A plausible explanation of the long-lasted (300–500 d; ∼1–1.5 yr) minimum of the X-ray emission from WR 48a could be that it is due to an occultation of the CSW X-ray emission by a very massive stellar wind (or a recently expelled LBV 'shell').

As discussed by Zhekov et al. (2014), the increased X-ray absorption near the maximum of the IR emission from WR 48a may indicate that the orbital inclination of this binary system is close to 90°. In such a case, we may expect to detect a primary maximum of the X-ray absorption when the WC8 component of the system is located between the CSW region and the observer. We note that the available data show that WR 48a was bright in X-rays on a considerably long time-scale, e.g. 10–12 yr or so (see Section 3.5), but the X-ray observations were scarce and we may have missed that primary maximum of the X-ray absorption.

On the other hand, if the increased X-ray absorption is related to some LBV-like activity in WR 48a, having a quasi-period of 30–32 yr, then the high X-ray attenuation will be observed *only* during the time when a new LBV 'shell' is expelled.

We thus believe that future observations in various spectral domains will be very helpful for our understanding of the physical picture in this fascinating object WR 48a. Good quality, high-resolution, optical spectra, taken regularly on approximately 1-yr basis, will allow us to constrain the physical properties (wind parameters, luminosity, spectral type etc.) of the stellar components in this dusty WR star. These observations should be supplemented by optical photometry as well. Multifrequency radio observations with high sensitivity will help us reveal if a non-thermal radio source exists in WR 48a or the system is just a thermal radio source as the current observations show. Deep high-resolution X-ray spectra, taken with *Chandra*, are needed to follow the changes of the physical properties of the hot plasma that likely originates from CSWs in WR 48a. In addition, regular observations, as the ones carried out with *Swift*, are important as well for obtaining crucial information on the X-ray variability of WR 48a, correspondingly on the global geometry of this presumable binary (or of a higher hierarchy) system.

The data from such comprehensive observational studies can be used to model the global properties of the dusty WR star WR 48a in considerable detail. This modelling can be carried out by making use of the stellar atmosphere models (for the optical emission), hydrodynamic models of colliding stellar winds (X-ray and non-thermal radio emission, if the latter is detected) and detailed physical models of dust emission (IR emission). Such a global analysis of the physical characteristics of WR 48a will allow us to thoroughly test our understanding of the physics of massive stars.

5 CONCLUSIONS

In this paper, we presented an analysis of the WR 48a emission in different spectral domains. The basic results and conclusions from such a multiwavelength view on this dusty WR star are as follows.

(i) The optical spectrum of WR 48a is acceptably well represented by a sum of two spectra: of a WR star of the WC8 type and of a WR star of the WN8h type. The comparison of the WR 48a spectra from 2011–2012 and 1993 reveals that the optical emission is variable. This is indicated by the change of the EWs of some emission lines, the relative brightness of the WC8 and WN8h spectral components and the optical extinction to this object.

(ii) Analysis of the interstellar absorption features in the spectra of WR 48a and the near-by stars D2-3 (2MASS J13125770−6240599) and S1 (D2-7; 2MASS J13125864−6240552) showed that these objects are at about the same distance from us. Keeping in mind that D2-3 and S1 are members of the open cluster Danks 2, we conclude that WR 48a is located at the distance of ∼4 kpc to Danks 1 and 2 (e.g. Danks et al. 1983; Davies et al. 2012).

(iii) WR 48a is very likely a thermal radio source and shows some variability on a time-scale of a few years or so. The level of the radio emission suggests a relatively high mass-loss rate of this dusty WR star ($\dot{M} \approx$ a few $\times\ 10^{-4}$ $M_\odot$ yr^{-1}).

(iv) Analysis of the data from different X-ray observatories (*Chandra*, *ROSAT*, *XMM–Newton*) revealed that WR 48a was a very bright X-ray source for an appreciably long period of time (e.g. 10–12 yr or so). Observations with *Swift* have now established its variability on a shorter time-scale (within 1–3 yr).

(v) The results from our multiwavelength view on the dusty WR star WR 48a in conjunction of the ones from the in-detail studies of its IR emission (Williams et al. 2012) and of its X-ray spectra (Zhekov et al. 2011, 2014) show that colliding stellar winds likely play a very important role in the physics of this object. However, the global physical picture in WR 48a may not be that simple and some LBV-like activity could not be excluded as well.

(vi) Future observations of WR 48a, taken on a regular time-basis along the entire spectral domain, from radio to X-ray, will be very helpful for our understanding of the physics of this fascinating WR star. In-detail modelling of this global data set will allow us to thoroughly test our understanding of the physics of massive stars.

ACKNOWLEDGEMENTS

This paper uses observations made at the South African Astronomical Observatory (SAAO). The corresponding data were obtained with the Southern African Large Telescope (SALT) and the Radcliffe telescopes. It is also based on observations made with NTT telescope at the La Silla Observatory, ESO, under programme ID: 087.D-0490A. The paper is also partly based on data from the ESO Science Archive Facility (under request numbers 110999, 111361 and 111364) and from the Anglo-Australian Telescope data archive. The Australia Telescope Compact Array is part of the Australia Telescope which is funded by the Commonwealth of Australia for operation as a National Facility managed by CSIRO. This research has made use of data and/or software provided by the High Energy Astrophysics Science Archive Research Center (HEASARC), which is a service of the Astrophysics Science Division at NASA/GSFC and the High Energy Astrophysics Division of the Smithsonian Astrophysical Observatory. This research has made use of the NASA's Astrophysics Data System, and the SIMBAD astronomical data base, operated by CDS at Strasbourg, France. JB and RK are supported by the Ministry of Economy, Development, and Tourism's Millennium Science Initiative through grant IC12009, awarded to The Millennium Institute of Astrophysics (MAS) and Fondecyt Reg. No. 1120601 and No. 1130140. The authors are grateful to the referee, Peredur Williams, for the valuable comments and suggestions.

REFERENCES

Abbott D. C., Bieging J. H., Churchwell E., Torres A. V., 1986, ApJ, 303, 239
Anders E., Grevesse N., 1989, Geochim. Cosmochim. Acta, 53, 19
Arnaud K. A., 1996, in Jacoby G., Barnes J., eds, ASP Conf. Ser. Vol. 101, Astronomical Data Analysis Software and Systems. Astron. Soc. Pac., San Francisco, p. 17
Bell A. R., 1978, MNRAS, 182, 147
Buckley D. A. H., Swart G. P., Meiring J. G., 2006, Proc. SPIE, 6267, 62670Z
Burgh E. B., Nordsieck K. H., Kobulnicky H. A., Williams T. B., O'Donoghue D., Smith M. P., Percival J. W., 2003, Proc. SPIE, 4841, 1463
Chené A.-N. et al., 2012, A&A, 545, 54
Crawford S. M. et al., 2010, Proc. SPIE, 7737, 773725
Danks A. C., Dennefeld M., Wamsteker W., Shaver P. A., 1983, A&A, 118, 301
Danks A. C., Wamsteker W., Shaver P. A., Retallack D. S., 1984, A&A, 132, 301
Davies B. et al., 2012, MNRAS, 419, 1871
Dougherty S. M., Williams P. M., 2000, MNRAS, 319, 1005
Dougherty S. M., Beasley A. J., Claussen M. J., Zauderer B. A., Bolingbroke N. J., 2005, ApJ, 623, 447
Fitzpatrick E. L., 1999, PASP, 111, 63
Hindson L., Thompson M. A., Urquhart J. S., Faimali A., Clark J. S., Davies B., 2012, MNRAS, 421, 3418
Høg E. et al., 2000, A&A, 355, L27
Jacoby G. H., Hunter D. A., Christian C. A., 1984, ApJS, 56, 257
Kobulnicky H. A., Nordsieck K. H., Burgh E. B., Smith M. P., Percival J. W., Williams T. B., O'Donoghue D., 2003, Proc. SPIE, 4841, 1634
Koenigsberger G., Georgiev L., Hillier D. J., Morrell N., Barba R., Gamen R., 2010, AJ, 139, 2600
Le Borgne J.-F. et al., 2003, A&A, 402, 433
McGregor P. J., Hyland A. R., Hillier D. J., 1988, ApJ, 324, 1071
McGruder C. H., 1975, A&AS, 22, 161
Mauerhan J. C., Van Dyk S. D., Morris P. W., 2009, PASP, 121, 591
Moorwood A., Cuby J. G., Lidman C., 1998, Messenger, 91, 9
O'Donoghue D. et al., 2006, MNRAS, 372, 151
Panagia N., Felli M., 1975, A&A, 39, 1
Pollock A. M. T., Corcoran M. F., Stevens I. R., Williams P. M., 2005, ApJ, 629, 482
Press W. H., Teukolsky S. A., Wettering W. T., Flannery B. P., 1992, Numerical Recepies in C: The Art of Scientific Computing. Cambridge Univ. Press, Cambridge
Pych W., 2004, PASP, 116, 148
Torres A. V., Massey P., 1987, ApJS, 65, 459
van der Hucht K. A., 2001, New Astron. Rev., 45, 135
van der Hucht K. A., Cassinelli J. P., Williams P. M., 1986, A&A, 168, 111

White R. L., Becker R. H., 1995, ApJ, 451, 352
Williams P. M., 1995, in van der Hucht K. A., Williams P. M., eds, Proc. IAU Symp. 163, Wolf-Rayet Stars: Binaries, Colliding Winds, Evolution. Kluwer, Dordrecht, p. 335
Williams P. M., van der Hucht K. A., Pollock A. M. T., Florkowski D. R., van der Woerd H., Wamsteker W., 1990, MNRAS, 243, 662
Williams P. M. et al., 2001, MNRAS, 324, 156
Williams P. M., van der Hucht K. A., Morris P. W., Marang F., 2003, in van der Hucht K. A., Herrero A., Esteban C., eds, Proc. IAU Symp. 212, A Massive Star Odyssey, from Main Sequence to Supernova. Astron. Soc. Pac., San Francisco, p. 115
Williams P. M., van der Hucht K. A., van Wyk F., Marang F., Whitelock P. A., Bouchet B., Setia Gunawan D. Y. A., 2012, MNRAS, 420, 2026
Wright A. E., Barlow M. J., 1975, MNRAS, 170, 41
Zhekov S. A., Skinner S. L., 2000, ApJ, 538, 808
Zhekov S. A., Gagné M., Skinner S. L., 2011, ApJ, 727, L17
Zhekov S. A., Gagné M., Skinner S. L., 2014, ApJ, 785, 8

APPENDIX A: THE SALT SPECTRA OF OTHER STARS

As was noted in Section 2.1, the long-slit mode of the SALT RSS spectrograph permitted us to obtain spectra of four additional stars S1, S2, S3 and S4, simultaneously with the spectra of WR 48a and D2-3. The SALT spectra of CPD-62 3058, a B star in close vicinity to WR 48a, were obtained with the same set-up on 2012 May 24. All these objects are marked in Fig. 1 and their spectra were reduced and analysed in the same way as described in Section 2.1. Some information for these objects is given in Table A1. The EWs of the interstellar lines and DIBs in their spectra are presented in Table A2.

An attempt to fit the observed spectra and to estimate the interstellar extinction was made by the use of the tasks FITGRID and FITSPEC in the STSDAS SYNPHOT[10] package. First, we ran FITGRID to find the best match to each of our spectra from the libraries of standard spectra. We then used FITSPEC with two free variables, *vegamag* in V passband and the $E(B-V)$ colour excess, for a more refined fit to our spectra. We note that the *vegamag* parameter is just a scaling factor for the fit and has no specific physical meaning since the SALT spectra are flux calibrated in relative units (see Section 2.1). The templates used were from the libraries of Jacoby, Hunter & Christian (1984) and Le Borgne et al. (2003). The spectra of Jacoby et al. (1984) cover the wavelength range 3510–7427 Å at a resolution of approximately 4.5 Å and are included in the STSDAS package. The spectra in the STELIB (Le Borgne et al. 2003) cover the range 3200–9200 Å with a resolution $\lesssim$3 Å. The fits to the spectra of CPD-62 3058, S1 and S2 are shown in Figs A1–A4. The spectra of the stars S3 and S4 were not fitted because of the low S/N ratio.

For the S1 star, which is a member of the open cluster Danks 2 (Davies et al. 2012), the strength of the interstellar absorption features in its spectrum is very similar to that in the spectra of D2-3 and WR 48a (see Table 3). This is a solid indication that all the three objects are located at about the same distance from us. Also, the interstellar extinction to S1 is consistent with that to D2-3 ($E(B-V) = 2.73$ versus 2.67 mag; see Section 3.3.1), which gives additional confidence for the results from our spectral fits.

The relatively small values of the interstellar extinction derived for CPD-62 3058 and S2 indicate that these objects are likely foreground stars. We note that the $E(B-V)$ value for CPD-62 3058 is in acceptable correspondence with that ($E(B-V) = 1.01$ mag) reported by McGruder (1975). The situation with the stars S3 and S4 is inconclusive because of the quality of their SALT spectra (see also Table A2).

APPENDIX B: GLOBAL SPECTRAL FITS TO THE WR 48a OPTICAL SPECTRA

The adopted technique for the global spectral fits to the optical spectra of WR 48a was discussed in Sections 3.3 and 3.3.2. We only recall that a two-component fit was used in this analysis. Since WR 48a was classified as WR star of the WC8 type, the first component of the fit was the SALT spectrum of the WC8 star D2-3 whose spectrum was derived simultaneously with that of WR 48a (see Section 2 and Fig. 1). For the second component in the WR 48a fit, we used spectra from STELIB library (Le Borgne et al. 2003) or from the archives of various observatories. The SALT and AAT spectra were fitted as the interstellar extinction was also taken into account. Another important parameter derived in the fits is the relative brightness of the stellar components. This is denoted by the difference of the intrinsic V magnitude of the WC8 star ($V_{\rm WC8}$) and its companion star ($V_{\rm C}$): $\Delta V = V_{\rm C} - V_{\rm WC8}$.

The results from these global fits were presented in Section 3.3.2 in the case of a WN8h spectrum as a second spectral component. These fits gave the best match to the optical SALT and AAT spectra of WR 48a. Fig. B1 presents some results from the global fits if the second component is a spectrum of a LBV, O or B star, respectively. We see that these fits are not able to match well the relatively narrow spectral lines of helium and hydrogen (He I 5876, 6678 Å, Hα 6563 Å). On the other hand, these fit results confirm one of the basic findings discussed in Section 3.3.2. Namely, the interstellar extinction in the SALT spectrum (2012 May) of WR 48a is higher than in its AAT spectrum (1993 June). They also establish the relative variability (change) between the strengths of the WC8 spectral component and that of the companion star.

[10] STSDAS is a product of the Space Telescope Science Institute, which is operated by AURA for NASA. Also, see http://www.stsci.edu/institute/software_hardware/stsdas/synphot/SynphotManual.pdf

Table A1. List of other stars observed with SALT.

Object name	2MASS	V (mag)	Spectral type[c]
B (CPD-62 3058)	J13123927−6243048	10.77[a]	B3
S1 (D2-7)	J13125864−6240552	15.91[b]	O8
S2	J13124234−6242379	15.12[b]	G0
S3	J13124037−6242518		
S4	J13123545−6243221		

[a] Høg et al. (2000); [b]NOMAD; [c]as derived here from the spectral fits.

Table A2. Interstellar absorption features in the spectra of CPD-62 3058, S1, S2, S3 and S4.

λ	CPD-62 3058	S1	S2	S3	S4
5780	0.57 ± 0.01				
5797	0.16 ± 0.01				
Na I 5889	0.72 ± 0.01	1.13 ± 0.03	1.03 ± 0.05[a]	2.14 ± 0.09[a]	1.34 ± 0.09[a]
Na I 5995	0.62 ± 0.01	1.04 ± 0.04	0.77 ± 0.04[a]	1.78 ± 0.10[a]	1.12 ± 0.11[a]
6283	1.56 ± 0.01	2.83 ± 0.06			
6614	0.18 ± 0.01	0.44 ± 0.03			
K I 7699	0.20 ± 0.03	0.36 ± 0.03	0.36 ± 0.07	0.60 ± 0.13	

Note. Given are the absorption line identification or the DIB wavelength (λ) in Å and its EW in Å for CPD-62 3058, S1, S2, S3 and S4, respectively.
[a]Likely blended with a stellar line.

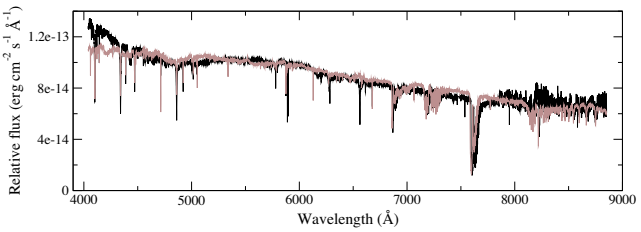

Figure A1. The STELIB library (Le Borgne et al. 2003) spectrum (in light brown) of HD 271163 (B3Ia), reddened by $E(B-V) = 0.74$ mag and fitted to the SALT spectrum (in black) of CPD-62 3058.

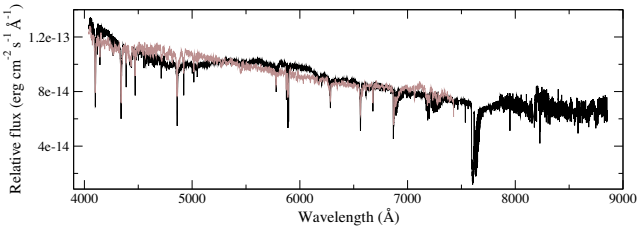

Figure A2. The Jacoby et al. (1984) library spectrum (in light brown) of HD 166125 (B3III), reddened by $E(B-V) = 0.76$ mag and fitted to the SALT spectrum (in black) of CPD-62 3058.

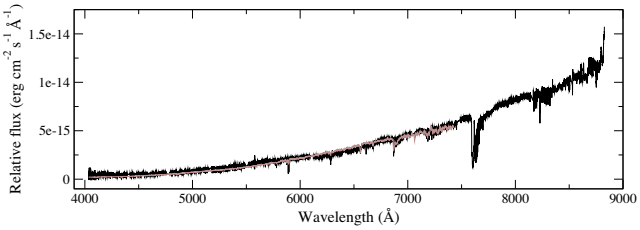

Figure A3. The Jacoby et al. (1984) library spectrum (in light brown) of HD 236894 (O8V), reddened by $E(B-V) = 2.73$ mag and fitted to the SALT spectrum (in black) of S1.

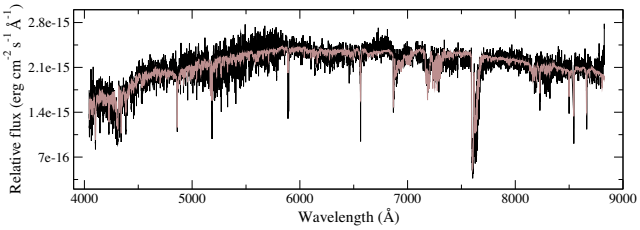

Figure A4. The STELIB library (Le Borgne et al. 2003) spectrum (in light brown) of HD 63077 (G0V), reddened by $E(B-V) = 0.46$ mag and fitted to the SALT spectrum (in black) of S2.

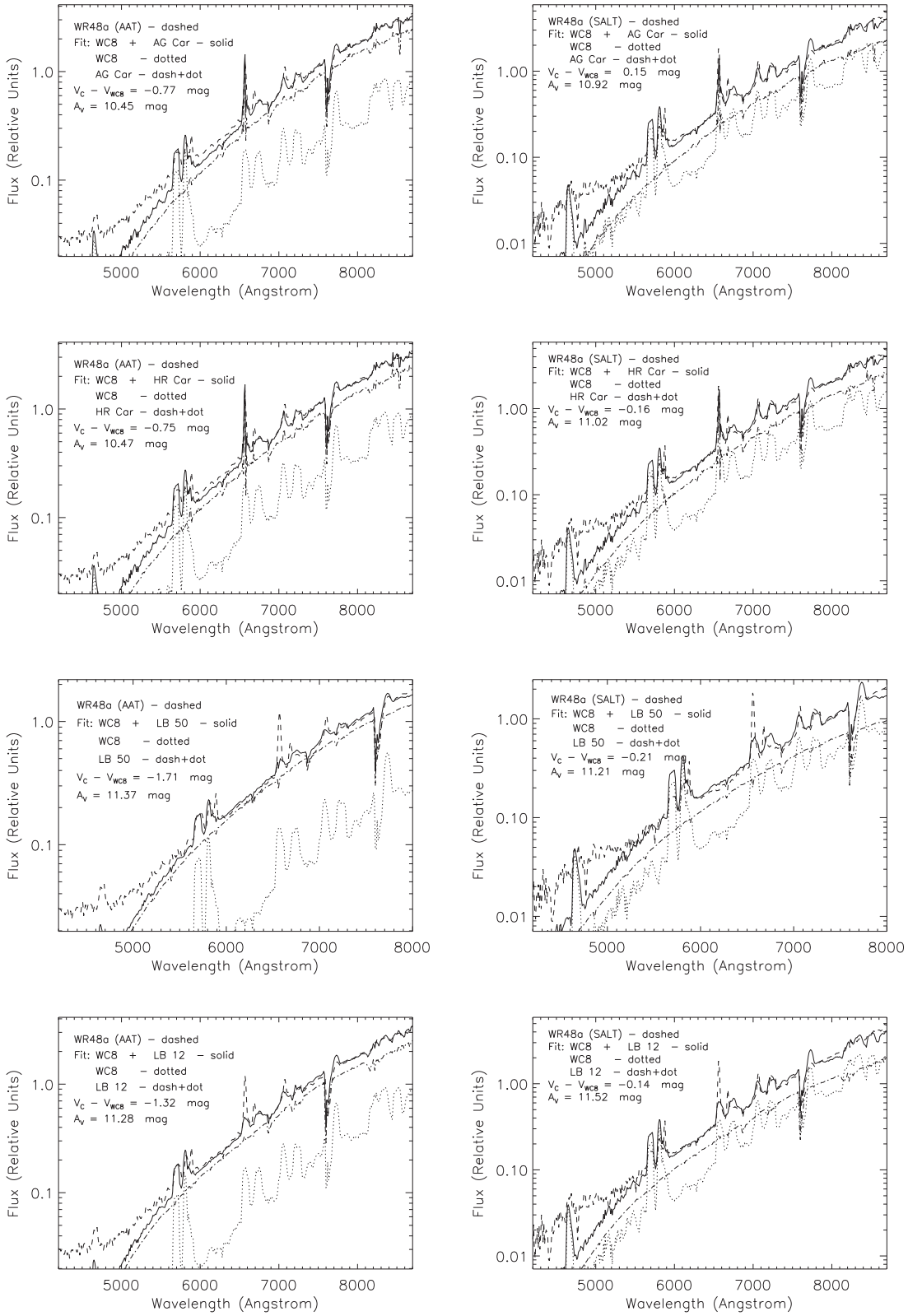

Figure B1. Examples of the two-component fits to the AAT and SALT spectra of WR 48a. The first component is the SALT spectrum of the D2-3 star and the second component is the spectrum of a LBV star (AG Car, HR Car), an O star (O5e; LB 50) and a B star (B2Ia; LB 12). The 'LB' denotes that the data are from the STELIB library of stellar spectra (Le Borgne et al. 2003). The two digits represent the object number in the library. The bin size is 10 Å.

This paper has been typeset from a TEX/LATEX file prepared by the author.